Surface Science 707 (2021) 121807

Contents lists available at ScienceDirect

Surface Science

journal homepage: www.elsevier.com/locate/susc

Synthesis of a planar, multicomponent catalytic surface of Na_2CO_3/MnO

Xu Feng [a,b,*], David F. Cox [a]

[a] Department of Chemical Engineering, Virginia Polytechnic Institute and State University, Blacksburg, VA 24061, USA
[b] Department of Chemistry, Virginia Polytechnic Institute and State University, Blacksburg, VA 24061, USA

ARTICLE INFO

Keywords:
Sodium oxide
Sodium carbonate
Manganese oxide
Oxygen exchange
X-ray photoelectron spectroscopy
Temperature programmed desorption

ABSTRACT

O_2 adsorption on MnO(100) precovered with sodium (Na) multilayers was investigated by X-ray photoelectron spectroscopy (XPS) and temperature programmed desorption (TPD). Deposition of Na multilayers leads to a first monolayer of oxidic Na followed by metallic Na island growth. XPS results for the oxidation of the metallic Na islands indicate an incomplete oxidation of Na at 125 K. Oxidation at 350 K completely oxidizes the metallic islands producing a mixture of Na_2O and Na_2O_2. Thermal evolution of the oxidation products was examined. After oxidation at 350 K and flashing to 750 K, Na_2O and Na_2O_2 are the primary oxides on MnO(100). After flashing to 850 K, a solid state reaction of Na_2O_2/Na_2O and the MnO(100) substrate forms a $NaMnO_2$-like surface compound which decomposes above 850 K. Oxygen exchange between CO_2 and Na oxides is observed. The strong interaction between CO_2 and Na oxide islands forms Na_2CO_3 on MnO(100). Heating the Na_2CO_3 covered MnO(100) surface to 600 K for 10 min drives oxidic Na in the first monolayer into the MnO subsurface, and produces a surface exposing islands of Na_2CO_3 on MnO(100).

1. Introduction

A novel low-temperature, manganese-oxide-based, catalytic thermochemical water splitting cycle has been reported by Xu, Bhawe and Davis [1]. This cycle starts by heating a powder mixture of Mn_3O_4 and Na_2CO_3 at 850 °C to produce MnO, $NaMnO_2$, Na_2CO_3 and release CO_2, then the hydrogen and oxygen evolution from water are driven by the redox cycle of manganese oxides between MnO and $NaMnO_2$. In the hydrogen evolution steps, it was found that Na_2CO_3 reacts with MnO in the presence of water at 850 °C to form $NaMnO_2$ and release hydrogen and CO_2. The authors proposed that Na_2CO_3 decomposes to release CO_2, while Na^+ intercalates into MnO to form α-$NaMnO_2$ where Mn^{2+} is oxidized to Mn^{3+} by water while accompanied by the release of hydrogen. It is our goal to utilize ultra-high vacuum surface science methodologies to build model surfaces to mimic the complex multicomponent catalysts to investigate the reaction mechanisms of hydrogen evolution in this innovative water splitting cycle.

To date we have made efforts to understand a number of key fundamental processes associated with the hydrogen evolution of the water splitting cycle, including the interaction between Na and MnO in a non-oxidizing environment [2] and the formation of $NaMnO_2$ from Na and MnO in the presence of O_2 and heat [3]. Starting with a well-defined MnO(100) single crystal, our study of Na deposition on MnO(100) in ultra-high vacuum [2] found that Na interacts strongly with the MnO substrate in an oxidic (Na^+) form up to 1 ML Na coverage. This form of Na is irreversibly-adsorbed and diffuses into the MnO bulk at elevated temperatures above 500 K. For Na coverages above 1 ML, metallic Na islands nucleate and grow on top of the oxidic Na monolayer and desorb from the surface at 430 K in TPD. Furthermore, annealing a surface precovered with 11.5 ML Na on MnO(100) in 1×10^{-6} Torr of O_2 at 673 K for 15 min followed by flashing to 1000 K in UHV produces a $NaMnO_2$-like surface [3]. These observations are in accordance with the mechanism proposed by Davis and co-workers [1] that Na intercalates into MnO to form $NaMnO_2$ in an oxidizing environment in the hydrogen evolution steps of the novel thermochemical water splitting cycle. In these studies, CO_2 has been used as a probe molecule to successfully distinguish the different forms of surface Na by their varying binding strength. It has been found that CO_2 interacts weakly with MnO(100) in the absence of Na and desorbs primarily below 200 K with a peak at 150 K and a minor broad desorption feature in the range of 200 – 500 K [2]. On the other hand, CO_2 binds strongly to both oxidic and metallic Na but with different strength. The interaction of CO_2 with oxidic Na in the first monolayer gives a CO_2 desorption feature at 650 K, while CO_2 bind stronger with metallic Na to give a CO_2 desorption feature at 735 K [2].

One of the remaining challenges has been to synthesize a model catalytic surface in ultra-high vacuum that resembles the

* Corresponding author.
E-mail address: xufeng@vt.edu (X. Feng).

https://doi.org/10.1016/j.susc.2021.121807
Received 8 October 2020; Received in revised form 14 December 2020; Accepted 22 January 2021
Available online 24 January 2021

multicomponent mixture of MnO and Na_2CO_3 that catalyzes the hydrogen evolution from water. With the knowledge we have gained in our previous studies above of the interaction of Na and MnO under several conditions, we have established a bottom-up approach to complete this task: a single crystal surface of MnO(100) is precovered with Na multilayers, then interacted with O_2 followed by CO_2 to form Na_2CO_3 islands on MnO(100). Most importantly, this surface needs to expose adsorption sites of Na_2CO_3, MnO, and interface sites between the two components in order to mimic the multicomponent nature of the catalyst in the novel water splitting cycle.

There have been a number of reports regarding the formation and characterization of sodium oxides and sodium carbonates on model surfaces. The oxidation of alkali metals has been investigated primarily for applications in heterogeneous catalysis [4-8], the oxidation of semiconductor surfaces [9-12] and cathode materials for electrochemical energy storage [13, 14]. The oxidation of alkali metals on metal substrates can give regular alkali metal oxide (M_2O), peroxide (M_2O_2) and superoxide (MO_2) which have been characterized by XPS O 1 s binding energies in the range of 527 - 531 eV, 531 - 533 eV and above 534 eV, respectively [15-17]. For the oxidation of Na on model surfaces, Na_2O and Na_2O_2 were formed by oxygen adsorption on Na-precovered Si(113) [18], while Na_2O overlayers were prepared by oxidation of Na-precovered Pd(100) [19].

Na_2CO_3 formation on model metal or metal oxide surfaces has been accomplished via two different reaction mechanisms. One method utilizes the interaction of CO_2 and Na_2O. Onishi et al. [19] oxidized Na-precovered Pd(100) to form Na_2O overlayers, with the adsorption of CO_2 on Na_2O thin films resulting in the formation of Na_2CO_3 on Pd(100). On TiO_2(110), deposited Na binds strongly to surface lattice oxygen of TiO_2 to form "Na_2O-dimer" units which sorb CO_2 to form carbonates [20]. A second approach is to directly expose metallic Na to CO_2. Seiferth et al. [21] studied CO_2 adsorption on Na-precovered Cr_2O_3(0001) at 90 K and found that CO_2 chemisorbs on Na, presumably in a $NaCO_2$ stoichiometry. Elevating the substrate temperature leads to a disproportionation reaction of chemisorbed CO_2 on Na to form Na_2CO_3 and release CO: $2NaCO_2 \rightarrow Na_2CO_3 + CO$. Similar disproportionation reactions and Na_2CO_3 formation were reported for CO_2 adsorption on Na-precovered Pd(111) [22], TiO_2(110) [23] and Fe_3O_4(111) [24].

In this work, the oxidation products of Na-precovered MnO(100) at 125 K and 350 K are identified. X-ray photoelectron spectroscopy (XPS) was used to characterize changes in chemical states of surface atoms. CO_2 was used as a probe molecule in temperature programmed desorption (TPD) to characterize the oxidized surfaces. Further thermal treatment of the oxidation products produces Na_2O, and the following CO_2 adsorption forms Na_2CO_3 on the MnO(100) substrate. Lastly, the synthetic procedure of the surface exposing both Na_2CO_3 and MnO is described.

2. Experimental

All experiments were carried out in a turbo-pumped, dual-chamber, stainless steel ultra-high vacuum (UHV) system. The preparation chamber with a base pressure of 2×10^{-10} Torr is equipped with a Leybold IQE 10/35 ion gun, a set of Princeton Research Instruments reverse view LEED optics and an Inficon Quaqrex 200 mass spectrometer for TPD. The analysis chamber with a base pressure of 1×10^{-10} Torr is equipped with a Leybold EA-11 hemispherical analyzer and a Mg Kα radiation source for XPS (1253.6 eV), and a Na evaporator with an SAES getter as the Na source.

The MnO(100) single crystal was purchased from SurfaceNet GmbH with an EPI polish. The crystal structure of MnO(100) has been described elsewhere [2]. The sample was mechanically clamped onto a Ta stage that was fastened to LN_2-cooled copper electrical feedthroughs in a sample rod manipulator. The sample temperature was directly measured by a type K thermocouple attached to the back of the single crystal through a hole in the Ta stage using Aremco 569 ceramic cement. The sample can be resistively heated to 1000 K and LN_2-cooled to 125 K. A heating rate of 2.5 K•s^{-1} was used in TPD. The low heating rate was used to avoid thermal-induced fracture of the ceramic MnO sample.

Na was evaporated onto the sample at 300 K from a resistively heated Na SAES getter placed approximately 30 mm away from the sample. O_2 (Matheson, 99.998%), $^{18}O_2$ (Linde Specialty Gases, >97 atom% ^{18}O, 99.9%) and $^{13}CO_2$ (Sigma-Aldrich, 99 atom% ^{13}C, < 3 atom% ^{18}O) were used as received. Gases were introduced by backfilling the chamber through a variable leak valve, and the reported exposures have been corrected for an ion gauge sensitivity of 1.4 for CO_2 and 1.0 for O_2 [25].

XPS spectra were acquired at 60 eV pass energy for Mn, O and Na 1 s which gives a Ag $3d_{5/2}$ line width of 1.06 eV, and 200 eV pass energy for Na KLL which gives a Ag $3d_{5/2}$ line width of 2.1 eV. C 1 s photoemission spectra overlap with the much more intense Na KLL features, thus no useful information was obtained concerning the nature of carbon for adsorbed CO_2. All binding energies have been referenced to an O 1 s binding energy of 530.1 eV for the MnO(100) substrate using an approach similar to that of Langell et al. [26]. This value was obtained with the sample at an elevated temperature of 473 K which provides sufficient conductivity to eliminate surface charging. The XPS spectra of the surface oxidized at 125 K (Fig. 1b) were taken at 125 K, and all others were taken at 300 K. XPSPEAK 4.1 software [27] was used for XPS peak fitting of O 1 s spectra. A 100% Gaussian peak profile was applied to obtain best fits for all O 1 s peaks using the Chi-squared method.

A clean and nearly-stoichiometric MnO(100) surface was prepared by ion bombardment at elevated temperature (Ar^+ bombardment, 2 KeV, 1000 K) and annealing to 1000 K in UHV to completely remove previously deposited Na as described elsewhere [2]. After the preparation procedure, the sample exhibits a sharp (1 × 1) LEED pattern characteristic of a simple termination of the rocksalt-structured (cubic) MnO bulk. This surface gives a Mn $2p_{3/2}$ binding energy of 641.0 eV, with a satellite feature at 6.2 eV higher binding energy. Both values are in good agreement with previous reports for a clean and stoichiometric MnO(100) surface [26]. A Mn 3 s splitting of 6.1 eV is also observed which also agrees with values reported for MnO [28-34]. XPS gives an *uncorrected* O 1 s to Mn 2p intensity ratio of 0.24, which matches the value for a clean and stoichiometric MnO(100) surface reported by Langell et al. [26].

3. Results and discussion

For each oxidation experiment, 3 ML of Na was deposited on MnO (100) which leads to both oxidic Na in the first monolayer and metallic Na islands [2]. O_2 exposures of 200 L (1 L ≡ 1×10^{-6} Torr•s) were used for subsequent oxidation. Two oxidation temperatures, 125 K and 350 K, were examined as routes for the formation of Na_2O on MnO(100). The surface oxidized at 350 K was also flashed to consecutively higher temperatures to characterize the thermal evolution of the oxidation products by XPS. TPD after oxidation was used to further characterize the thermal evolution of the oxidation products. In addition, CO_2 TPD was used to probe the surface Na species after oxidation at 350 K and subsequent thermal treatments.

3.1. XPS

3.1.1. Na oxidation at 125 K

Fig. 1(a) shows the XPS spectra of the MnO(100) precovered with 3 ML of Na. Binding energy values for surfaces in Fig. 1 are summarized in Table 1. The single O 1 s peak at 530.1 eV arises from the lattice oxygen of the underlying MnO substrate. The appearance of plasmon loss features in both Na 1 s and Na KLL spectra indicates the presence of metallic Na on MnO(100) [35-38]. The Mn $2p_{3/2}$ binding energy of 641.1 eV and the satellite feature at 647.3 eV are similar to those for clean MnO(100) and are characteristic of Mn^{2+}. These results are consistent with our previous study [2].

Fig. 1(b) shows the XPS spectra of a 3 ML Na precovered MnO(100)

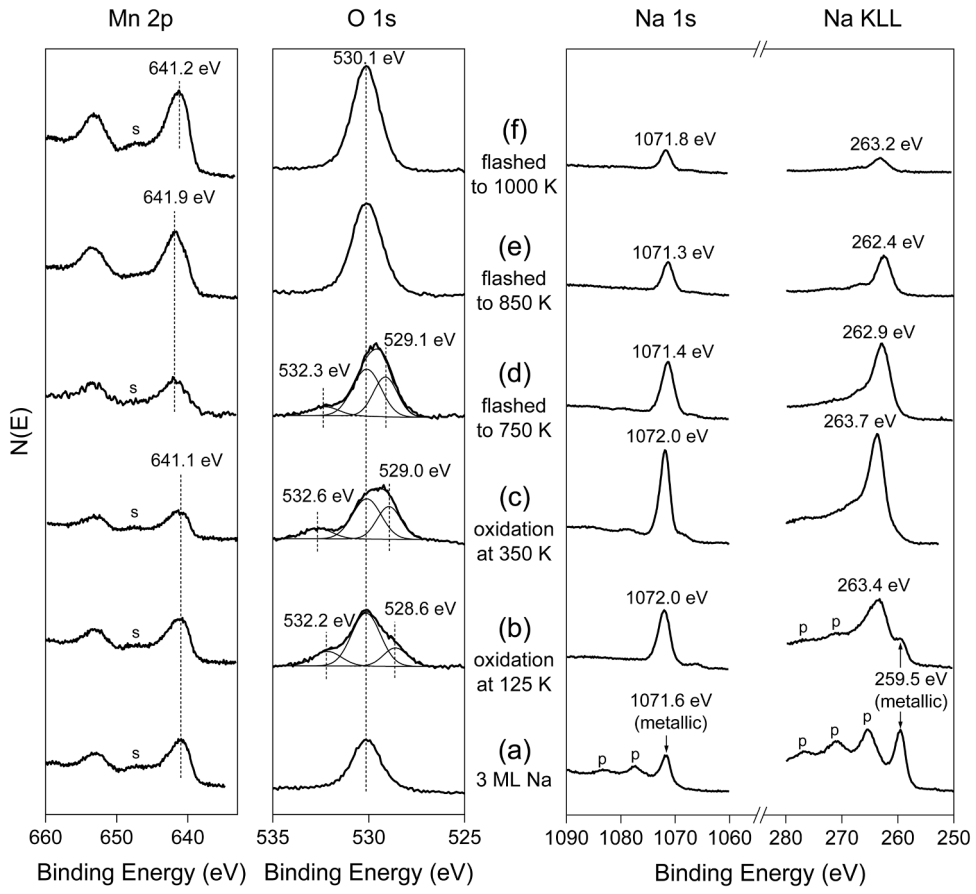

Fig. 1. Mn 2p, O 1 s, Na 1 s and Na KLL XPS spectra of (a) 3 ML Na precovered MnO(100); (b) surface a followed by a 200 L O_2 exposure at 125 K; (c) surface a followed by a 200 L O_2 exposure at 350 K; (d) surface c after flashing to 750 K; (e) surface c after flashing to 850 K; (f) surface c after flashing to 1000 K. Symbol p represents plasmon loss features for metallic Na. Symbol s represents the shake-up satellite feature of Mn $2p_{3/2}$ that is characteristic of Mn^{2+}.

Table 1
Summary of XPS binding energy values for the prepared surfaces in Fig. 1.

Sample/BE (eV)	Mn $2p_{3/2}$ peak	Mn $2p_{3/2}$ satellite	O *1s*	Na *1s*	Na *KLL*
3 ML Na	641.1	647.3	530.1	1071.6	259.5
oxidation at 125 K	641.1	647.3	528.6	1072.0	263.4
			530.1		
			532.2		
oxidation at 350 K	641.1	647.3	529.0	1072.0	263.7
			530.1		
			532.6		
flashed to 750 K	641.9	647.3	529.1	1071.4	262.9
			530.1		
			532.3		
flashed to 850 K	641.9	–	530.1	1071.3	262.4
flashed to 1000 K	641.2	647.4	530.1	1071.8	263.2

surface after exposure to 200 L of O_2 at 125 K. The Na 1 s binding energy shifts to 1072.0 eV, and a new Na KLL feature appears at 263.4 eV. No plasmon loss features are observed in Na 1 s spectra indicating the absence of metallic Na, however in the Na KLL spectra the feature at 259.5 eV and plasmon loss features characteristic of metallic Na are greatly attenuated but still present. The Na 1 s binding energy shifts to a higher value by 0.4 eV compared to that for metallic Na, which is close to the reported 0.7 eV increase for the oxidation of metallic Na to Na_2O [35, 37, 39]. The 3.9 eV increase of the new Na KLL feature at 263.4 eV compared to that for metallic Na (259.5 eV) is also similar to reports for Na oxidation to Na_2O [37]. Therefore, we conclude that Na oxides such as Na_2O are formed by the oxidation of metallic Na at 125 K. The appearance of plasmon loss features in the Na KLL spectra but not in the Na 1 s spectra can be attributed to the difference in the mean free paths of the emitted electrons. Given that Na 1 s features are more surface sensitive than those for Na KLL because of their lower kinetic energy (higher binding energy), the difference in the Na features indicate that the surface of the metallic Na islands is oxidized upon interacting with O_2 at 125 K, while the inner core retains some metallic Na due to the limited mobility of Na and O atoms at 125 K. Thus an incomplete oxidation of the metallic Na islands occurs at 125 K.

In the O 1 s spectra, besides the main peak at 530.1 eV attributed to the lattice oxygen in the MnO substrate, two shoulder features are observed at 532.2 eV and 528.6 eV, indicating that two different Na oxidation products were formed. Hwang et al. [18] deposited Na on a Si (113) wafer followed by O_2 exposures at 150 K. Two O 1 s peaks presumably from Na oxidation products were observed by XPS at 532.6 and 528.8 eV, which were attributed to Na_2O_2 and Na_2O respectively. Similarly, Krix and Nienhaus [17] studied the interaction between O_2 and Na/Si(001) at 120 K using XPS and concluded that Na_2O_2 (533.0 eV) and Na_2O (529.2 eV) are the two Na oxidation products. Therefore, we assign the O 1 s feature at 528.6 eV to Na_2O, and the other O 1 s shoulder at 532.2 eV to Na_2O_2.

In summary, an incomplete oxidation of the metallic Na islands on MnO(100) occurs at 125 K, giving a mixture of Na_2O_2 and Na_2O. No obvious change in the Mn $2p_{3/2}$ binding energy is observed compared to that for the clean MnO(100), indicating no significant change in the Mn oxidation state (2+).

3.1.2. Na oxidation at 350 K

Oxidation of Na-precovered MnO(100) was also performed at 350 K in an attempt to enhance the oxidation of metallic Na to Na_2O. It was

found in our previous work [2] that at an elevated substrate temperature of 350 K in UHV, metallic Na is stable and does not desorb from MnO (100) in TPD, and no thermally-induced chemical change is observed for the deposited Na as characterized by XPS, thus making this temperature suitable for the oxidation of Na-precovered MnO(100). In addition, Onishi et al. [19] were able to prepare Na_2O overlayers on Pd(100) by repeatedly depositing Na on the substrate followed by O_2 exposure at 350 K.

Fig. 1(c) shows the XPS spectra of the 3 ML Na-precovered MnO(100) surface after exposure to 200 L of O_2 at 350 K. Compared to the 125 K oxidation results in Fig. 1(b), the binding energy of Na 1 s stays the same, while the Na KLL peak shifts slightly by +0.3 eV to 263.7 eV. The absence of plasmon loss features indicates that all the metallic Na has been oxidized. The O 1 s spectra shows two shoulder features at 532.6 and 529.0 eV along with the lattice oxygen in MnO at 530.1 eV, which are all similar to those on the surface prepared at 125 K. We again assign the O 1 s feature at 532.6 eV to Na_2O_2 and the O 1 s feature at 529.0 eV to Na_2O. In comparison to the data for oxidation at 125 K, the peak area ratio of Na_2O:Na_2O_2 increases significantly from 1.1 at 125 K to 2.7 at 350 K, indicating that the formation of Na_2O is favored over Na_2O_2 upon the oxidation of Na-precovered MnO(100) at 350 K. Additionally, the peak area ratio of Na_2O_2:lattice O shows no obvious change (0.27 at 125 K and 0.25 at 350 K), while the ratio of Na_2O:lattice O increases from 0.29 at 125 K to 0.68 at 350 K. These results suggest that the Na_2O formation is greatly enhanced at higher oxidation temperatures, and are consistent with the complete oxidation of metallic Na at 350 K.

In summary, a complete oxidation of metallic Na islands on MnO (100) is observed at 350 K, and is thought to give a mixture of Na_2O_2 and Na_2O.

3.1.3. Thermal evolution of the Na oxidation products

A thermal treatment involving the sequential heating of the oxidized surface to successively higher temperatures in UHV was used to examine the thermal evolution of the oxidation products. After oxidation at 350 K and flashing to 750 K (Fig. 1d), both of the O 1 s shoulder features in Fig. 1(c) are observed at 532.3 and 529.1 eV respectively, indicating that the mixture of Na_2O_2 and Na_2O formed at 350 K are still present on the sample surface after flashing to 750 K. The peak area ratio of Na_2O:Na_2O_2 increases from 2.7 at 350 K to 3.8 after flashing to 750 K, while the ratio of (Na_2O+Na_2O_2):lattice O only shows a slight drop from 0.94 at 350 K to 0.90 after flashing to 750 K, suggesting that a fraction of Na_2O_2 has been reduced to Na_2O upon heating to 750 K. On the other hand, the Na 1 s and Na KLL binding energies shift to lower values at 1071.4 eV and 262.9 eV respectively, indicating a change in the chemical environment of Na. The Mn $2p_{3/2}$ binding energy shifts to a higher value of 641.9 eV which is characteristic of Mn^{3+} [3], while the Mn $2p_{3/2}$ satellite peak for Mn^{2+} is still present but barely visible, indicating that a significant portion of Mn on the sample surface have been oxidized from Mn^{2+} to Mn^{3+}. Therefore, we suggest that the majority of the formed mixture of Na_2O_2 and Na_2O are intact at 750 K, while a solid state reaction involving the MnO substrate and Na_2O_2/-Na_2O has started at their interfaces.

After flashing to 850 K (Fig. 1e), the binding energies of Na 1 s at 1071.3 eV and Na KLL at 262.4 eV both match values observed for $NaMnO_2$ prepared on MnO(100) by a different approach in our previous work [3]. The Mn $2p_{3/2}$ binding energy of 641.9 eV characteristic of Mn^{3+} [3] is observed and the Mn $2p_{3/2}$ satellite peak for Mn^{2+} is completely gone, consistent with the expected Mn^{3+} oxidation state in $NaMnO_2$. Therefore, we conclude that $NaMnO_2$ is present on MnO(100) after flashing to 850 K. Given that the O 1 s features at 532.3 eV for Na_2O_2 and 529.1 eV for Na_2O are both absent in Fig. 1(e), we suggest that $NaMnO_2$ is formed via a solid state reaction of Na_2O_2/Na_2O and MnO. In the reported thermochemical water splitting cycle [1], a reaction of Na_2CO_3 and MnO in the presence of water gives $NaMnO_2$ and CO_2, while water is reduced to hydrogen. The solid state reaction of Na_2O and MnO to form $NaMnO_2$ observed in this work suggests a similar reaction, given that Na_2O is a likely reaction product from the decomposition of Na_2CO_3 to release CO_2.

In our previous work on the formation of $NaMnO_2$ by a different approach [3], a $NaMnO_2$-like surface formed by the oxidation of 11.5 ML of Na on MnO(100) decomposes upon heating to 1000 K in UHV for more than 10 min. After flashing the surface in Fig. 1(e) to 1000 K (Fig. 1f), the Na 1 s and KLL binding energies are similar to those obtained after the decomposition of $NaMnO_2$ in our previous work [3], and the Mn $2p_{3/2}$ binding energy shifts to 641.2 eV with the re-appearance of a satellite peak which are characteristic of Mn^{2+}. Therefore, we suggest the $NaMnO_2$ formed by a solid state reaction between Na_2O_2/Na_2O and MnO thermally decomposes above 850 K.

3.2. TPD after Na oxidation

TPD traces following a 200 L O_2 dose on the 3 ML Na-precovered MnO(100) surface at 125 K and 350 K are shown in Fig. 2. In the TPD traces from the surface oxidized at 125 K (Fig. 2a), no direct desorption of sodium oxide species such as Na_2O_2 ($m/z = 78$) or Na_2O ($m/z = 62$) was detected. A low temperature O_2 desorption feature is observed below 400 K, and a broad O_2 desorption signal is present above 620 K. A sharp Na desorption feature is observed at 420 K, and a broad Na desorption signal is present between 690 K and 820 K.

The low-temperature O_2 features below 400 K may be associated with desorption of excess oxygen not fully incorporated into the sodium oxides either from adsorbed molecular O_2 or recombination of O adatoms. The broad high temperature O_2 desorption above 620 K is attributed to the thermal decomposition of Na_2O_2/Na_2O. Na desorption at 420 K is similar to the desorption of metallic Na at 430 K as described in our previous work [2], indicating the presence of metallic Na on the surface, and is consistent with the incomplete oxidation of metallic Na at 125 K observed in XPS. The high temperature Na desorption between 690 K and 820 K is in the same temperature range as that for the high temperature O_2 desorption above 620 K, consistent with the thermal decomposition of Na_2O_2/Na_2O. We note that the high temperature O_2 and Na desorption traces represent a small fraction of the total amount of surface oxygen and Na. The desorbed amount of O_2 is less than that from a 0.1 L dose of O_2 on clean MnO(100) at 125 K, and the amount of desorbed Na is equivalent to only about 0.16 ML of metallic Na by comparison to our earlier work [2]. This result suggests that a majority of Na_2O_2/Na_2O reacts with MnO to form $NaMnO_2$ above 750 K, as characterized by XPS.

In the TPD traces from the surface oxidized at 350 K (Fig. 2b), no Na desorption is observed around 430 K indicating no metallic Na is present

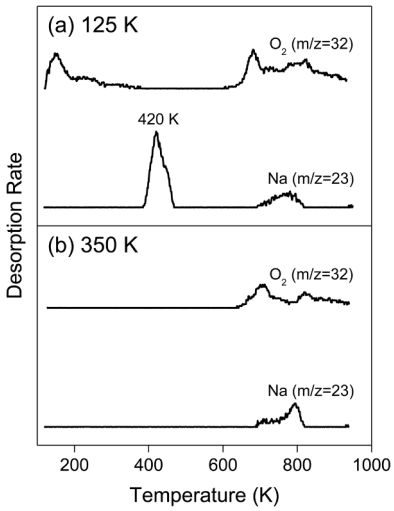

Fig. 2. TPD traces of O_2 ($m/z = 32$) and Na ($m/z = 23$) following a 200 L O_2 exposure on a 3 ML Na precovered MnO(100) surface at (a) 125 K; (b) 350 K.

on the surface, consistent with the complete oxidation of metallic Na at 350 K observed in XPS. O_2 desorption above 640 K and Na desorption between 690 K and 820 K are observed, both similar to those in Fig. 2(a) which have been attributed to the thermal decomposition of Na_2O_2/Na_2O.

3.3. CO_2 TPD

CO_2 was used as a probe molecule to characterize surface sodium species after oxidation at 350 K and thermal treatment at higher temperatures in UHV. After each surface was prepared, it was cooled to 125 K before $^{13}CO_2$ exposure, then TPD was run for the temperature range from 125 K to 1000 K. ^{18}O-labeled O_2 was used for the oxidation treatments in this section to generate ^{18}O-containing sodium oxide surface species. Monitoring oxygen exchange between $^{13}CO_2$ and ^{18}O-labeled surface oxide species characterized by TPD traces of $^{13}C^{16}O_2$ (no exchange), $^{13}C^{16}O^{18}O$ (single exchange) and $^{13}C^{18}O_2$ (double exchange) can provide information about the binding of CO_2 on the surface oxide species.

Fig. 3(a) shows the TPD traces of $^{13}CO_2$ ($m/z = 45$) and ^{13}CO ($m/z = 29$) from the surface precovered with 2.33 ML of Na with metallic Na present (no oxidation) as described in our previous work [2]. The strong binding of CO_2 with metallic Na gives rise to a broad, high temperature $^{13}CO_2$ desorption feature at 735 K. Just under 20% of the CO_2 adsorbed on metallic Na goes through a disproportionation reaction [21]: $2NaCO_2 \rightarrow Na_2CO_3 + CO$ as evidenced by the broad ^{13}CO signal between 450 K and 800 K.

Fig. 3(b) shows the CO_2 TPD traces from a 3 ML Na precovered MnO (100) surface after oxidation with 200 L of $^{18}O_2$ at 350 K. A high temperature CO_2 desorption feature at 800 K is observed with a smaller peak at 705 K. For both features, oxygen exchange is observed with a similar ratio of 0.2:0.5:0.3 for $^{13}C^{16}O_2$ (no exchange):$^{13}C^{16}O^{18}O$ (single exchange):$^{13}C^{18}O_2$ (double exchange). No CO desorption signal is detected. If a similarly prepared surface is first flashed to 750 K before CO_2 adsorption (Fig. 3c), the CO_2 desorption feature at 705 K in Fig. 3(b) is absent, while the feature at 800 K is present but attenuated. A ratio of 0.2:0.5:0.3 for $^{13}C^{16}O_2$ (no exchange):$^{13}C^{16}O^{18}O$ (single exchange):$^{13}C^{18}O_2$ (double exchange) is observed for the 800 K feature, similar to what was seen in Fig. 3(b). A low temperature CO_2 desorption feature near 150 K is also observed, and a small, broad CO_2 desorption feature is present from 200 K to 500 K. No CO desorption signal is detected.

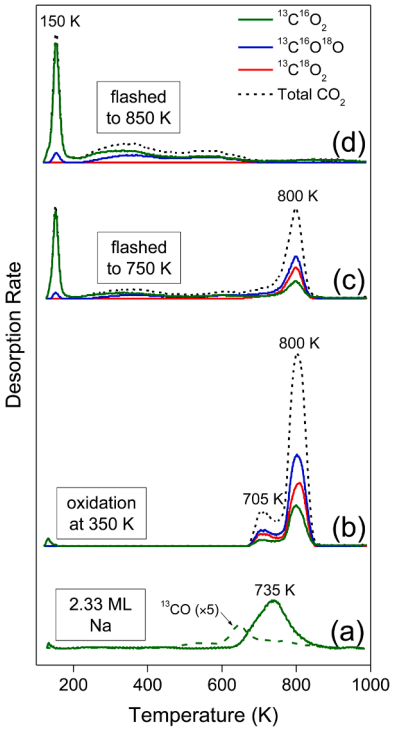

Fig. 3. TPD traces following a 0.5 L $^{13}CO_2$ exposure on (a) 2.33 ML Na precovered MnO(100); (b) 3 ML Na precovered MnO(100) followed by a 200 L of O_2 exposure at 350 K; (c) surface b after flashing to 750 K; (d) surface b after flashing to 850 K. (For interpretation of the references to colour in this figure legend, the reader is referred to the web version of this article.)

Since a mixture of Na_2O and Na_2O_2 are the expected products following oxidation at 350 K as identified by XPS, the high temperature CO_2 desorption features at 705 K and 800 K in Fig. 3(b) are attributed to the strong binding of CO_2 to the sodium oxides, Na_2O and Na_2O_2. After flashing to 750 K, only the 800 K CO_2 desorption feature is present, however the XPS results indicate that both Na_2O_2 and Na_2O remain present following this treatment. Therefore, we cannot attribute the appearance of the two CO_2 desorption features at 705 and 800 K in Fig. 3 (b) individually to the two sodium oxides, although they surely arise from different CO_2 binding sites on the sodium oxides or at their interface with the MnO. We note that the temperature range of the 705 K feature also overlaps with the temperature for CO_2 chemisorbed on metallic Na shown in Fig. 3(a). However, given that a complete oxidation of metallic Na occurs at 350 K as characterized by XPS and TPD after oxidation, a contribution from chemisorbed CO_2 on metallic Na is ruled out. Additionally, the absence of CO desorption indicates that no CO_2 disproportionation reaction occurs from adsorbed CO_2, again suggesting that no metallic Na is present.

The observation of oxygen exchange between CO_2 and surface oxides is an indication of carbonate formation [40-43]. Oxygen exchange has been reported between CO_2 and several metal oxides such as MgO [40-43] and Al_2O_3 [44]. It has been reported that when the MgO(100) surface is exposed to CO_2, bidentate carbonate must be present after CO_2 adsorption in order for an oxygen exchange (single and double) to occur [40-43], with C in CO_2 bonding to a surface O, and an O in CO_2 bonding to an adjacent surface Mg [40, 41, 43]. Fig. 4 (reproduced with permission from Ref. [43]) illustrates the proposed three migration processes for bidentate CO_2 on MgO(100) that can lead to single and double oxygen exchange of CO_2 [41, 43]. In process (I) CO_2 rolls over the surface without breaking any C—O bond, while in process (II) one of the C—O bond in CO_2 breaks when the C atom forms a bond with the adjacent surface O atom. Process (III) does not involve any C—O bond

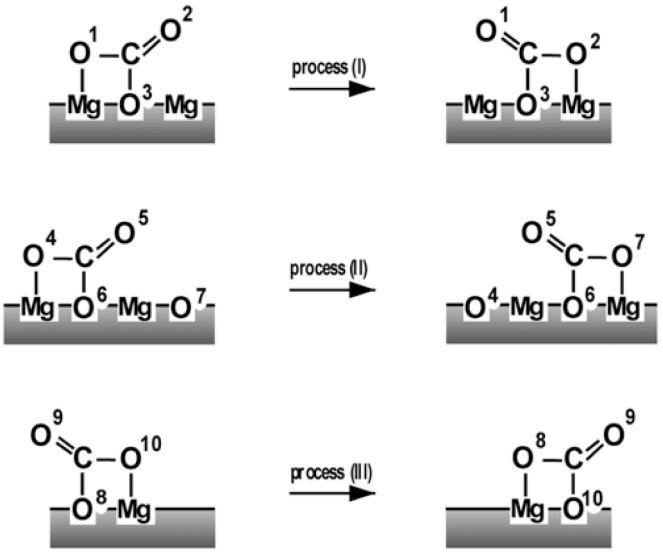

Fig. 4. Illustration of the proposed mechanism for single and double oxygen exchange between CO_2 and MgO(100) in Ref. [41, 43]. Reprinted with permission from Scheme 1 in Ref. [43]. Copyright (2003) American Chemical Society.

breaking, but rather the trading of an O atom between CO_2 and MgO (100) during the CO_2 migration. A single oxygen exchange occurs in process (II) or (III), and the repetition of process (I), (II) and (III) result in a double oxygen exchange. Since significant oxygen exchange is observed in CO_2 desorption features from Na_2O and Na_2O_2 in TPD (Fig. 3b), we conclude that Na_2CO_3 is formed by the interaction between CO_2 and Na_2O and Na_2O_2, and decomposes to give CO_2 desorption features at 705 K and 800 K in Fig. 3(b). We note that while C 1 s XPS can generally be used to characterize changes in chemical states of surface carbon to distinguish between molecularly adsorbed CO_2 and carbonate, the C 1 s signal in this work overlaps with the much more intense features of Na KLL spectra, thus no usable information about the carbonate formation is obtained from C 1 s XPS measurements.

The low temperature CO_2 desorption feature near 150 K and the small, broad CO_2 desorption feature from 200 K to 500 K after flashing to 750 K (Fig. 3c) are similar to the CO_2 TPD features observed from terraces and defects of MnO(100) respectively [45]. This result suggests a partially exposed MnO(100) surface, which can be formed by the inward diffusion of the oxidic Na in the first monolayer that occurs above 500 K as seen in our previous work [2]. We note that the small amount of $^{13}C^{16}O^{18}O$ (6%) at 150 K is due to the uptake of background CO_2 at $m/z = 47$ which is observed in the chamber after multiple isotope-exchange experiments.

If a Na-precovered surface is oxidized and flashed to 850 K prior to CO_2 exposure (Fig. 3d), a CO_2 desorption feature at 150 K and broad CO_2 desorption features from 200 K to 700 K are observed, similar to those on either a $NaMnO_2$-like surface [3] or the partially exposed MnO(100) in Fig. 3(c). The CO_2 desorption feature at 800 K in Fig. 3(c) is not observed. Since this CO_2 desorption feature at 800 K has been attributed to the decomposition of Na_2CO_3 formed by the reaction of CO_2 and Na_2O_2/Na_2O, its absence indicates the absence of surface Na_2O_2/Na_2O after flashing to 850 K, and is consistent with the suggestion of a solid state reaction between Na_2O_2/Na_2O and MnO(100) to form $NaMnO_2$ near 850 K as proposed from the XPS data.

3.4. Synthesizing a surface exposing both Na_2CO_3 and MnO

In the reported thermochemical water splitting cycle [1], water splits to produce hydrogen over a mechanical mixture of Na_2CO_3 and MnO. Modeling such a multicomponent catalytic system is thought to be important for gaining insight into the reaction mechanisms of hydrogen evolution, but can be challenging when starting with a single crystal MnO substrate in UHV.

In this work, efforts have been made to produce a surface exposing both Na_2CO_3 and MnO(100) to model the multicomponent surface of Na_2CO_3/MnO. With the knowledge obtained about the interactions between Na, O_2, CO_2 and MnO from our previous and current studies, a bottom-up approach is proposed to achieve the goal with a controlled 4-step surface reaction. Fig. 5(a) to (d) are cartoons illustrating the morphology and composition of the surface as a function of the 4-step synthetic procedure, and the control parameters and rationality are described below. The resulting surface is examined by CO_2 TPD and shown in Fig. 5(e).

Step 1 of the synthesis begins with a clean MnO(100) single crystal surface and the deposition of 3 ML of Na on MnO(100). It has been found in previous study of Na deposition on MnO(100) [2] that, for a multilayer Na coverage, oxidic Na is formed for the first monolayer of deposited Na, followed by the growth of metallic Na islands. The 3 ML Na precovered MnO(100) surface is illustrated in Fig. 5(a).

In the second step, the 3 ML Na precovered MnO(100) surface is exposed to 200 L of O_2 at 350 K. The metallic Na islands on MnO(100) are oxidized to form Na_2O and Na_2O_2, as confirmed by XPS in *Section 3.1*. Therefore, a MnO(100) surface covered with an oxidic Na monolayer and sodium oxide islands (Na_2O and Na_2O_2) is prepared as illustrated in Fig. 5(b).

In the third step, the resulting surface in Fig. 5(b) is exposed to CO_2 at

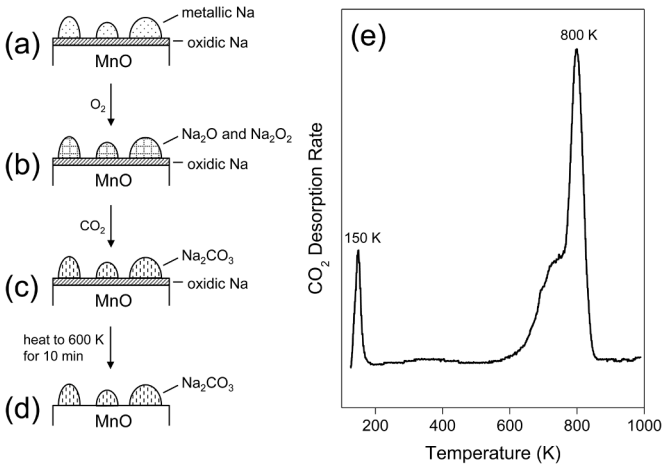

Fig. 5. (a) to (d): cartoons illustrating the morphology and composition of surfaces in the controlled 4-step synthetic procedure to produce a surface exposing Na_2CO_3 islands on MnO; (e) CO_2 TPD traces following a 0.5 L $^{13}CO_2$ dose on the synthesized surface (d) exposing Na_2CO_3 islands on MnO.

125 K. Sodium oxide (Na_2O and Na_2O_2) islands interact strongly with CO_2 and form Na_2CO_3 islands on MnO(100), as concluded from the CO_2 TPD results in *Section 3.3*. Therefore, a MnO(100) surface covered with an oxidic Na monolayer and Na_2CO_3 islands is prepared, as illustrated in Fig. 5(c).

The final step is to remove the oxidic Na monolayer between the Na_2CO_3 islands and the MnO(100) substrate without causing substantial damages to the Na_2CO_3 islands, providing both Na_2CO_3 and MnO sites in close proximity to model the multicomponent surface of Na_2CO_3/MnO. It has been found in previous work [2] that the oxidic Na in the monolayer can be driven into the MnO subsurface and bulk by heating to 600 K for 10 min in UHV, leaving an MnO surface with adsorption properties similar to pristine MnO(100). This temperature is high enough to remove chemisorbed CO_2 from the oxidic Na monolayer [2], and is considerably lower than that for the thermal decomposition of the majority of Na_2CO_3 around 800 K (as characterized by CO_2 TPD in *Section 3.3*) *or* the solid state reaction of Na_2O_2/Na_2O and MnO to form $NaMnO_2$ above 750 K (as characterized by XPS in *Section 3.1* and CO_2 TPD in *Section 3.3*). Therefore, heating the MnO(100) surface covered by an oxidic Na monolayer and Na_2CO_3 islands as illustrated in Fig. 5(c) to 600 K for 10 min in UHV should drive the oxidic Na monolayer into the MnO subsurface without introducing notable thermal changes to the Na_2CO_3 islands on top of it, thus producing a surface exposing Na_2CO_3 islands on MnO(100) as illustrated in Fig. 5(d).

CO_2 TPD was used to characterize the surface prepared by this 4-step synthetic procedure. TPD traces of $^{13}CO_2$ ($m/z = 45$) are shown in Fig. 5 (e) following a 0.5 L CO_2 dose on the synthesized surface at 125 K. A low temperature CO_2 desorption feature near 150 K is observed, along with a small, broad feature from 200 K to 500 K, and a high temperature CO_2 desorption feature at 800 K with a shoulder around 720 K. The CO_2 desorption feature at 150 K and the broad feature from 200 K to 500 K are similar to the desorption features from CO_2 adsorption on terraces and defects of MnO(100) respectively [2, 45], confirming the exposure of bare MnO(100). The CO_2 desorption feature at 800 K with a shoulder around 720 K is similar to the ones from the decomposition of Na_2CO_3 formed by the interaction between CO_2 and sodium oxides as characterized by CO_2 TPD in *Section 3.3*, indicating the presence of Na_2CO_3. A CO_2 desorption feature at 650 K representing the CO_2 desorption from the oxidic Na monolayer [2] is **not** observed, indicating that the oxidic Na monolayer between the Na_2CO_3 islands has been driven into the subsurface of MnO where it is no longer accessible to the CO_2 adsorbent. Therefore, we conclude that the 4-step synthetic procedure provides a surface exposing both Na_2CO_3 and MnO sites in close proximity to model

the multicomponent, catalytic surface of Na_2CO_3/MnO in the novel water splitting cycle.

4. Conclusion

A mixture of Na_2O_2 and Na_2O are formed by the oxidation of Na islands on MnO(100) at 125 K and 350 K. Na_2O_2/Na_2O reacts with the MnO(100) substrate to form $NaMnO_2$ below 850 K. CO_2 interacts strongly with Na_2O and Na_2O_2 to form Na_2CO_3. A surface exposing Na_2CO_3 islands on MnO(100) has been synthesized to model the complex Na_2CO_3/MnO multicomponent system used for hydrogen evolution in the reported thermochemical water splitting cycle [1].

Credit author statement

Xu Feng: Methodology, Investigation, Writing - Original Draft
David F. Cox: Funding acquisition, Conceptualization, Methodology, Writing - Review & Editing, Supervision

Declaration of Competing Interest

The authors declare that they have no known competing financial interests or personal relationships that could have appeared to influence the work reported in this paper.

Acknowledgment

The authors gratefully acknowledge financial support by the Chemical Sciences, Geosciences and Biosciences Division, Office of Basic Energy Sciences, Office of Science, U.S. Department of Energy through Grant DE-FG02-97ER14751, and private support from Mr. and Mrs. Lewis W. van Amerongen.

References

[1] B. Xu, Y. Bhawe, M.E. Davis, Low-temperature, manganese oxide-based, thermochemical water splitting cycle, Proc. Natl. Acad. Sci. 109 (2012) 9260–9264.
[2] X. Feng, D.F. Cox, Na Deposition on MnO(100), Surf. Sci. 645 (2016) 23–29.
[3] X. Feng, D.F. Cox, Oxidation of MnO(100) and $NaMnO_2$ formation: characterization of Mn^{2+} and Mn^{3+} surfaces via XPS and water TPD, Surf. Sci. 675 (2018) 47–53.
[4] J.G. Chen, M.D. Weisel, J.H. Hardenbergh, F.M. Hoffmann, C.A. Mims, R.B. Hall, Evidence for the potassium-promoted activation of methane on a K-doped NiO/Ni (100) surface, J. Vac. Sci. Technol. A 9 (1991) 1684–1687.
[5] E. Iwamatsu, T. Moriyama, N. Takasaki, K. Aika, Oxidative coupling of methane over Na^+- and Rb^+-doped MgO catalysts, J. Catal. 113 (1988) 25–35.
[6] E. Iwamatsu, K.-I. Aika, Kinetic analysis of the oxidative coupling of methane over Na^+-doped MgO, J. Catal. 117 (1989) 416–431.
[7] A. Machocki, A. Denis, Simultaneous oxidative coupling of methane and oxidative dehydrogenation of ethane on the Na^+/CaO catalyst, Chem. Eng. J. 90 (2002) 165–172.
[8] D.J. Wang, M.P. Rosynek, J.H. Lunsford, Oxidative coupling of methane over oxide-supported sodium-manganese catalysts, J. Catal. 155 (1995) 390–402.
[9] P. Soukiassian, T.M. Gentle, M.H. Bakshi, Z. Hurych, SiO_2-Si interface formation by catalytic oxidation using alkali metals and removal of the catalyst species, J. Appl. Phys. 60 (1986) 4339–4341.
[10] A. Franciosi, P. Philip, S. Chang, A. Wall, A. Raisanen, N. Troullier, P. Soukiassian, Electronic promoters and semiconductor oxidation: alkali metals on Si(111) surfaces, Phys. Rev. B 35 (1987) 910–913.
[11] E.G. Michel, E.M. Oellig, M.C. Asensio, R. Miranda, Alkali-induced oxidation of silicon, Surf. Sci. 189-190 (1987) 245–251.
[12] E.G. Michel, J.E. Ortega, E.M. Oellig, M.C. Asensio, J. Ferrón, R. Miranda, Early stages of the alkali-metal-promoted oxidation of silicon, Phys. Rev. B 38 (1988) 13399–13406.
[13] J. Desilvestro, O. Haas, Metal oxide cathode materials for electrochemical energy storage: a review, J. Electrochem. Soc. 137 (1990) 5C–22C.
[14] M.S. Whittingham, Lithium batteries and cathode materials, Chem. Rev. 104 (2004) 4271–4302.
[15] S.L. Qiu, C.L. Lin, J. Chen, M. Strongin, The formation of metal-oxygen species at low temperatures, J. Vac. Sci. Technol. A 8 (1990) 2595–2598.
[16] J. Jupille, P. Dolle, M. Besançon, Ionic oxygen species formed in the presence of lithium, potassium and cesium, Surf. Sci. 260 (1992) 271–285.
[17] D. Krix, H. Nienhaus, Low-temperature oxidation of alkali overlayers: ionic species and reaction kinetics, Appl. Surf. Sci. 270 (2013) 231–237.
[18] C.C. Hwang, K.S. An, R.J. Park, J.S. Kim, J.B. Lee, C.Y. Park, A. Kimura, A. Kakizaki, Bonding nature between oxygen and sodium on Si(113) surface, J. Vac. Sci. Technol. A 16 (1998) 1073–1077.
[19] H. Onishi, T. Aruga, Y. Iwasawa, Na_2O overlayers epitaxially prepared on Pd(100) and structure-sensitive CO_2 adsorption, Surf. Sci. 310 (1994) 135–146.
[20] H. Onishi, T. Aruga, C. Egawa, Y. Iwasawa, Active structures and electronic states for adsorption of CO_2 and NO on an Na/TiO_2(110) surface, J. Chem. Soc. Faraday Trans. 1 85 (1989) 2597–2604.
[21] O. Seiferth, K. Wolter, H. Kuhlenbeck, H.J. Freund, CO_2 adsorption on Na precovered Cr_2O_3(0001), Surf. Sci. 505 (2002) 215–224.
[22] J. Wambach, G. Odörfer, H.J. Freund, H. Kuhlenbeck, M. Neumann, Influence of alkali co-adsorption on the adsorption and reaction of CO_2 on Pd(111), Surf. Sci. 209 (1989) 159–172.
[23] J. Nerlov, S.V. Christensen, S. Weichel, E.H. Pedersen, P.J. Møller, A photoemission study of the coadsorption of CO_2 and Na on TiO_2(110)-(1×1) and -(1×2) surfaces: adsorption geometry and reactivity, Surf. Sci. 371 (1997) 321–336.
[24] J. Nerlov, S.V. Hoffmann, M. Shimomura, P.J. Møller, Coadsorption of Na and CO_2 on the Fe_3O_4(111) termination of α-Fe_2O_3(0001): relations between structure and activation, Surf. Sci. 401 (1998) 56–71.
[25] R.L. Summers, NASA Technical Note TN d-5285, Washington, D. C., 1969.
[26] M.A. Langell, C.W. Hutchings, G.A. Carson, M.H. Nassir, High resolution electron energy loss spectroscopy of MnO(100) and oxidized MnO(100), J. Vac. Sci. Technol. A 14 (1996) 1656–1661.
[27] R.W.M. Kwok, XPS Peak Fitting Program for WIN95/98 XPSPEAK Version 4.1, in, Department of Chemistry, The Chinese University of Hong Kong, Shatin, Hong Kong, 2000.
[28] V. Di Castro, G. Polzonetti, XPS study of MnO oxidation, J. Electron. Spectrosc. Relat. Phenom. 48 (1989) 117–123.
[29] F. Müller, R. de Masi, D. Reinicke, P. Steiner, S. Hüfner, K. Stöwe, Epitaxial growth of MnO/Ag(001) films, Surf. Sci. 520 (2002) 158–172.
[30] L.Z. Zhao, V. Young, XPS studies of carbon supported films formed by the resistive deposition of manganese, J. Electron. Spectrosc. Relat. Phenom. 34 (1984) 45–54.
[31] J.S. Foord, R.B. Jackman, G.C. Allen, An X-ray photoelectron spectroscopic investigation of the oxidation of manganese, Philos. Mag. A 49 (1984) 657–663.
[32] M. Oku, K. Hirokawa, S. Ikeda, X-ray photoelectron spectroscopy of manganese-oxygen systems, J. Electron. Spectrosc. Relat. Phenom. 7 (1975) 465–473.
[33] C.S. Fadley, D.A. Shirley, Multiplet splitting of metal-atom electron binding energies, Phys. Rev. A 2 (1970) 1109–1120.
[34] P. Steiner, R. Zimmermann, F. Reinert, T. Engel, S. Hüfner, 3s- and 3p-core level excitations in 3d-transition metal oxides from electron-energy-loss spectroscopy, Z. Phys. B: Condens. Matter 99 (1996) 479–490.
[35] H. Onishi, C. Egawa, T. Aruga, Y. Iwasawa, Adsorption of Na atoms and oxygen-containing molecules on MgO(100) and (111) surfaces, Surf. Sci. 191 (1987) 479–491.
[36] J.F. Moulder, W.F. Stickle, P.E. Sobol, K.D. Bomben, Handbook of X-ray Photoelectron Spectroscopy, Perkin-Elmer Corporation, Eden Prairie, MN, 1992.
[37] A. Barrie, F.J. Street, An Auger and X-ray photoelectron spectroscopic study of sodium metal and sodium oxide, J. Electron. Spectrosc. Relat. Phenom. 7 (1975) 1–31.
[38] M. Bender, K. Al-Shamery, H.J. Freund, Sodium adsorption and reaction on NiO (111)/Ni(111), Langmuir 10 (1994) 3081–3085.
[39] Y.C. Lee, P.A. Montano, J.M. Cook, An XPS study of the interaction of SO_2 with CaO(100): effect of temperature and metal adsorbates (Fe, Na), Surf. Sci. 143 (1984) 423–441.
[40] T. Shishido, H. Tsuji, Y. Gao, H. Hattori, H. Kita, Extensive oxygen exchange between carbon dioxide and magnesium oxide surface, React, Kinet. Catal. Lett. 51 (1993) 75–79.
[41] H. Tsuji, T. Shishido, A. Okamura, Y. Gao, H. Hattori, H. Kita, Oxygen exchange between magnesium oxide surface and carbon dioxide, J. Chem. Soc. Faraday Trans. 90 (1994) 803–807.
[42] Y. Yanagisawa, K. Takaoka, S. Yamabe, Exchange of strong carbon dioxide O=C bonds on an MgO surface, J. Chem. Soc. Faraday Trans. 90 (1994) 2561–2566.
[43] H. Tsuji, A. Okamura-Yoshida, T. Shishido, H. Hattori, Dynamic behavior of carbonate species on metal oxide surface: Oxygen scrambling between adsorbed carbon dioxide and oxide surface, Langmuir 19 (2003) 8793–8800.
[44] J.B. Peri, Oxygen exchange between $C^{18}O_2$ and "acidic" oxide and zeolite catalysts, J. Phys. Chem. 79 (1975) 1582–1588.
[45] X. Feng, H. Chen, D.F. Cox, CO_2 and Water Adsorption on MnO(100), Unpublished results.